Supporting Information

Van der Waals Heterojunction between Bottom-Up Grown Doped Graphene Quantum Dot and Graphene for Photoelectrochemical Water Splitting

Yibo Yan[a,e], Dong Zhai[b,c], Yi Liu[b], Jun Gong[e], Jie Chen[e], Ping Zan[e], Zhiping Zeng[e], Shuzhou Li[d], Wei Huang[a], Peng Chen[e]**

[a]Shaanxi Institute of Flexible Electronics, Northwestern Polytechnical University, 127 West Youyi Road, Xi'an 710072, China

[b]Materials Genome Institute (MGI), International Centre for Quantum and Molecular Structures (ICQMS), Department of Physics, Shanghai University, 333 Nanchen Road, Shanghai 200444, P. R. China

[c]Institute of Molecular Sciences and Engineering, Shandong University, 72 Binhai Road, Qingdao 266237, P. R. China

[d]School of Materials Science and Engineering, Nanyang Technological University, Singapore, 639798, Singapore

[e]School of Chemical and Biomedical Engineering, Innovative Centre for Flexible Devices, Nanyang Technological University, 70 Nanyang Drive, 637457, Singapore

*Corresponding Author:
Wei Huang: iamwhuang@nwpu.edu.cn
Peng Chen: ChenPeng@ntu.edu.sg

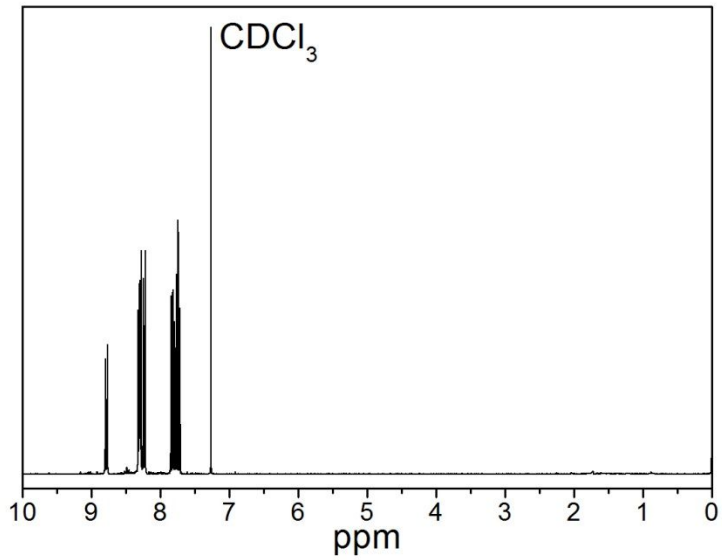

Figure S1. ^{1}H NMR of nitrated naphthalene which consists of 1-nitronaphthalene, 1,5-dinitronaphthalene and 1,8-dinitronaphthalene, using $CDCl_3$ as solvent.

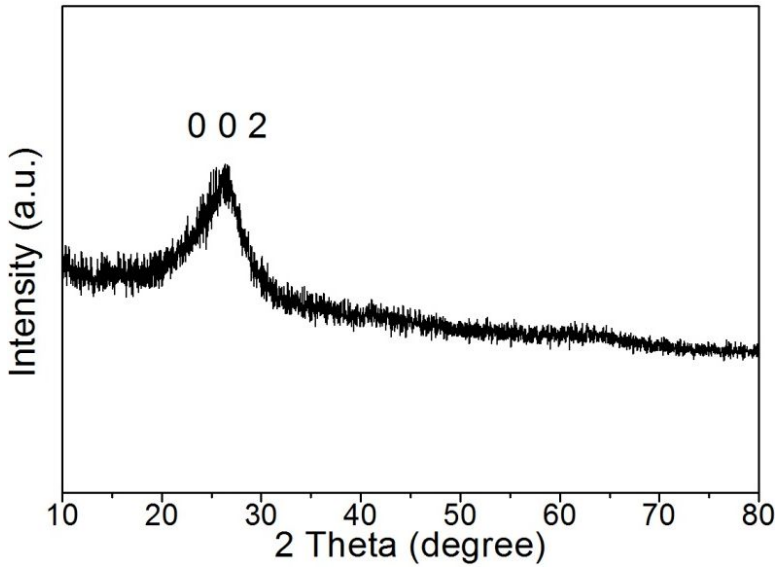

Figure S2. The XRD spectrum of GQDs synthesized from naphthalene.

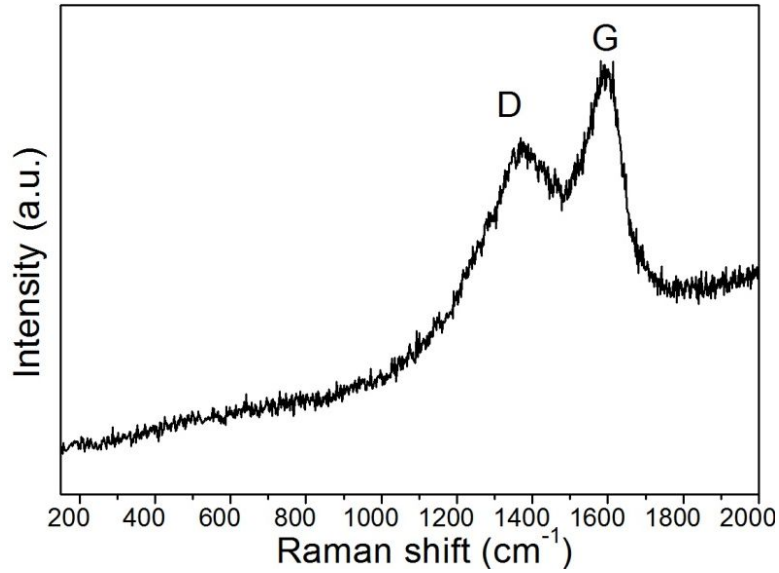

Figure S3. The Raman spectrum of GQDs synthesized from naphthalene. The ordered G band and disordered D band are located at 1580 cm^{-1} and 1370 cm^{-1}, respectively.

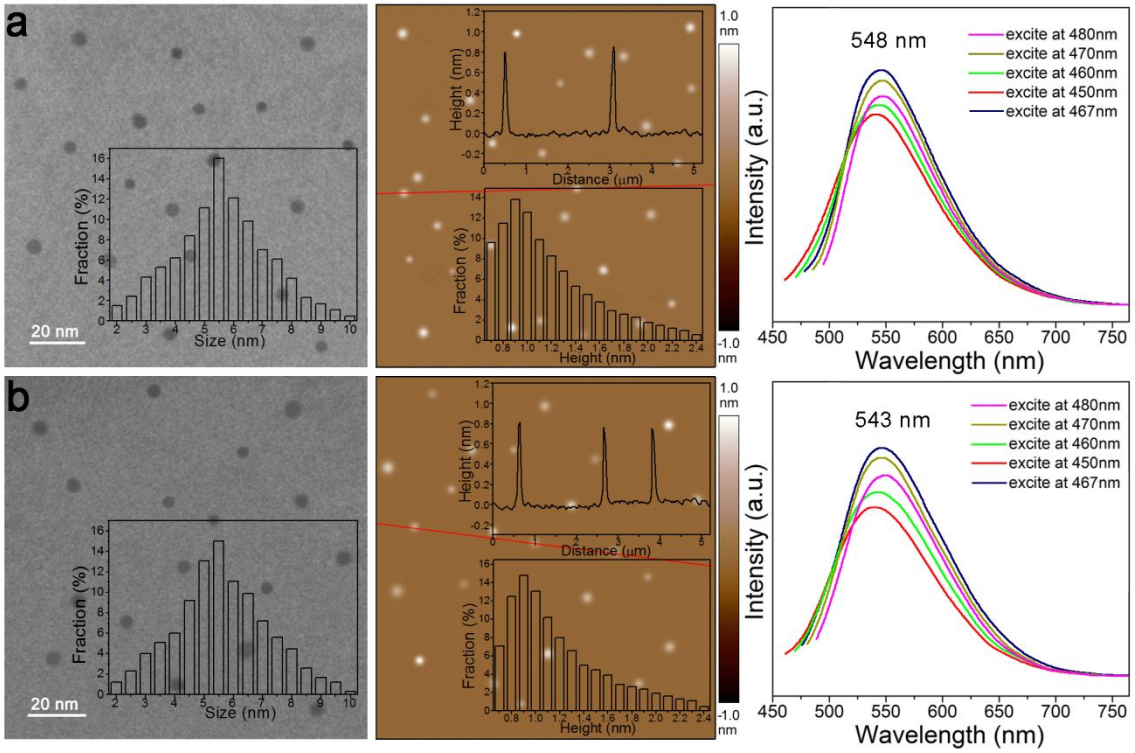

Figure S4. GQDs obtained using 1,5-dinitronaphthalene (a) or 1,8-dinitronaphthalene (b) as the precursor. (left column) TEM image and size distribution (GQDs obtained from 1,5-dinitronaphthalene: 5.64 ± 1.71 nm, n=134; GQDs obtained from 1,8-dinitronaphthalene: 5.61 ± 1.53 nm, n=142); (middle column) AFM image. Inset shows the height profile along the red-line and the height distribution (GQDs obtained from 1,5-dinitronaphthalene: 1.25 ± 0.46 nm, n=151; GQDs obtained from 1,8-dinitronaphthalene: 1.20 ± 0.41 nm, n=129); (right column) Photoluminescence spectra of GQD solution. 548 and 543 nm are the emission peaks at the best excitation of 467 nm for GQDs synthesized from 1,5-dinitronaphthalene and 1,8-dinitronaphthalene, respectively.

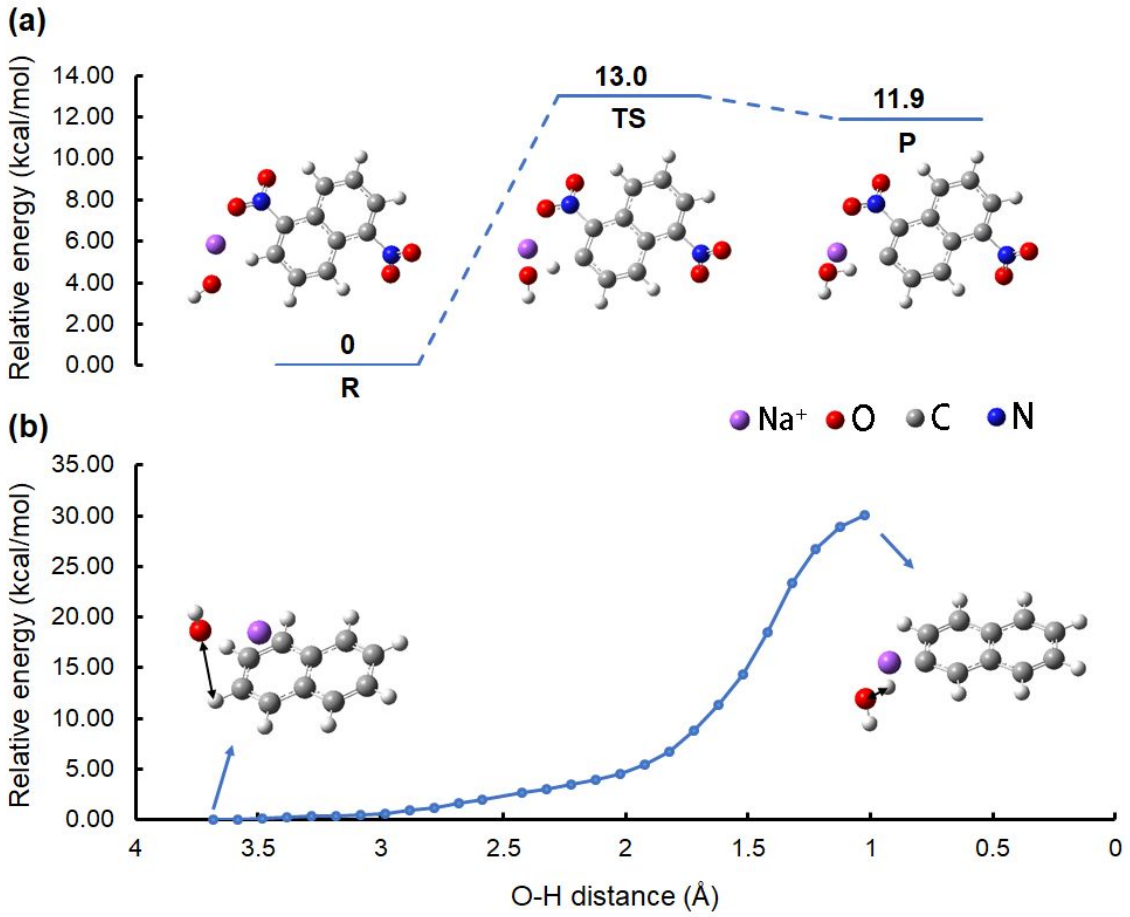

Figure S5. Reaction energy of dehydrogenation. (a) Calculated energy profile along reaction path of dehydrogenation of 1,5-dinitronaphthalene. (R=Reactant, TS=Transition state, P=Product) (b) Calculated reaction energy curve versus distance between O from OH^- and H from naphthalene (two atoms at the ends of the black arrow). The lack of minimum point on this curve means that such reaction cannot stably occur.

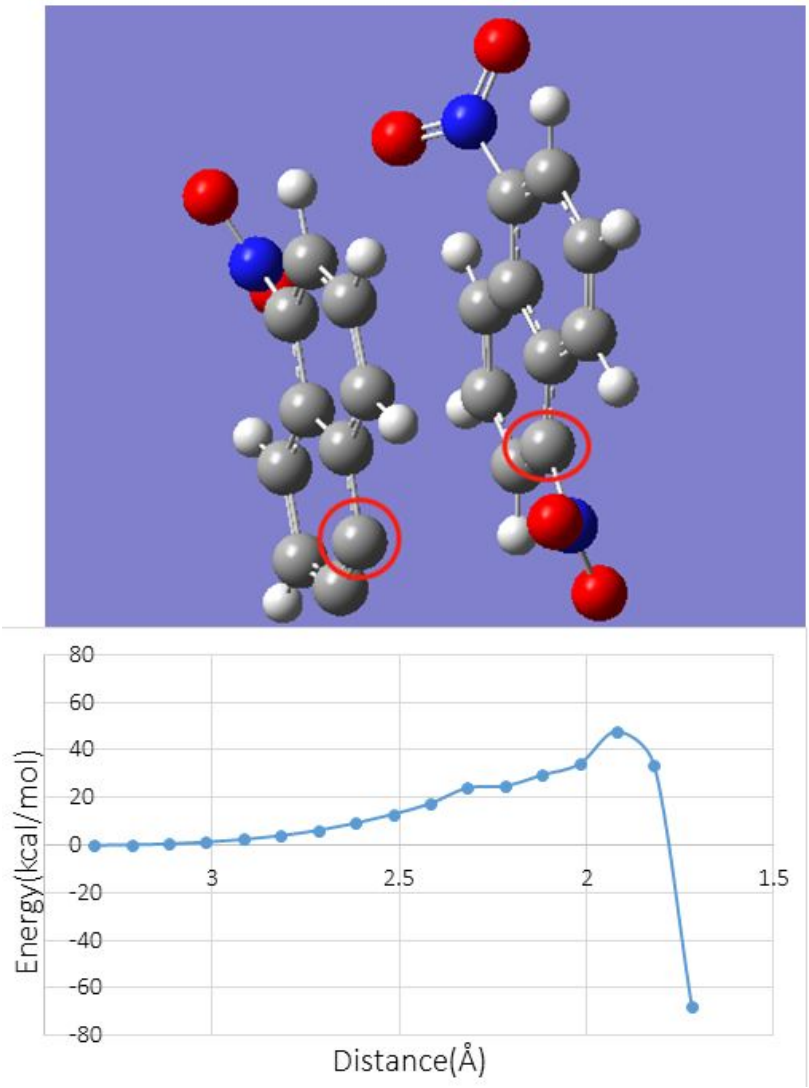

Figure S6. The energy barrier for naphthalene alkyne to attack the precursor (1,5-dinitronaphthalene) is as high as 50 kcal/mol.

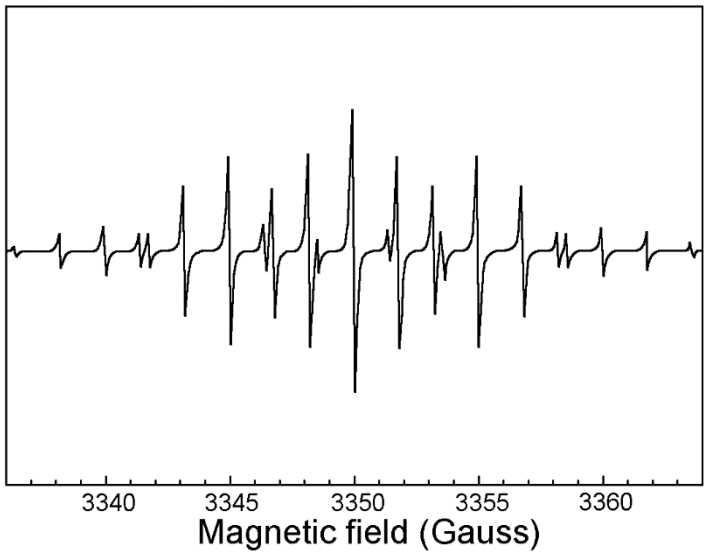

Figure S7. Electron paramagnetic resonance (EPR) spectrum of the intermediate naphthalene alkyne radical scavenged by TEMPO during the synthesis process, whose pattern is in consistence with the previously reported [1].

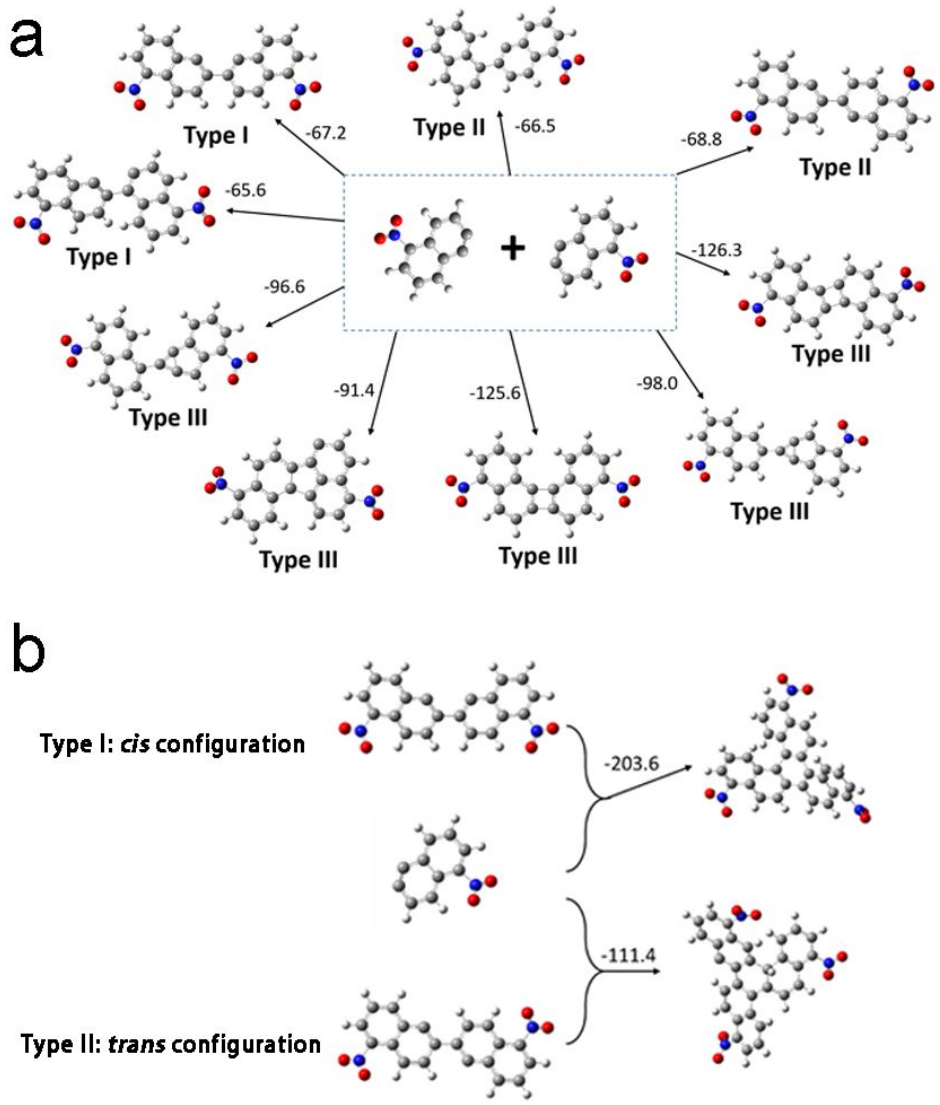

Figure S8. Fusion of naphthalene alkyne molecules. (a) Dimerization of two naphthalene alkyne molecules. (b) Trimer formation upon fusion between *cis* or *trans* dimers and naphthalene alkyne. The numbers have the unit of kcal/mol.

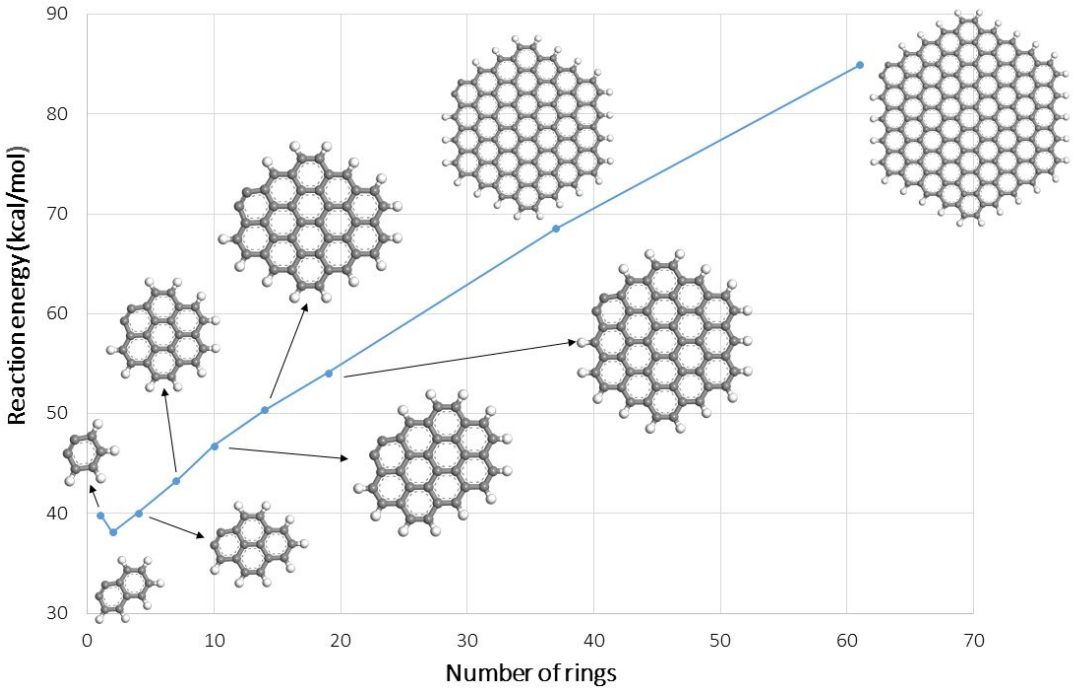

Figure S9. DFT calculated total energy barriers for one dehydrogenation plus one denitration reaction on GQDs with different sizes.

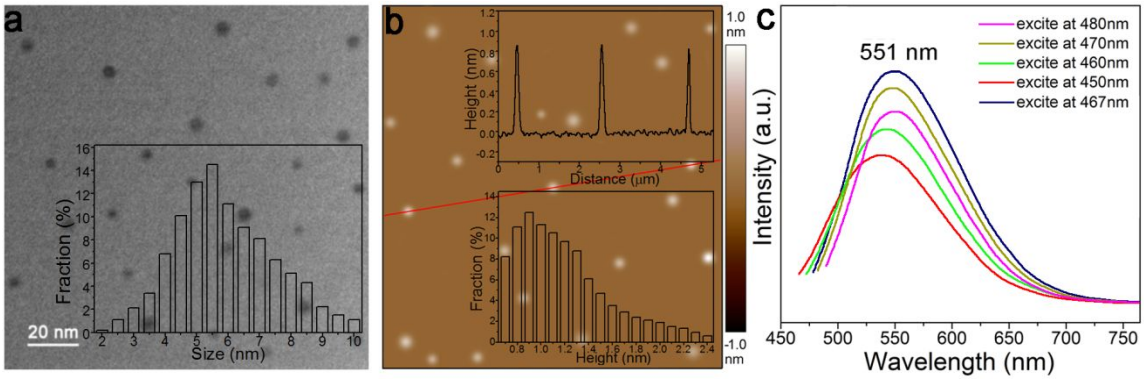

Figure S10. GQDs obtained with doubled reaction time (16 h). (a) TEM image and size distribution (5.91 ± 2.61 nm, n=148). (b) AFM image. Inset shows the height profile along the red-line and the height distribution (1.28 ± 0.56 nm, n=149). (c) Photoluminescence spectra of GQD solution. The 551 nm is the emission peak at the best excitation of 467 nm.

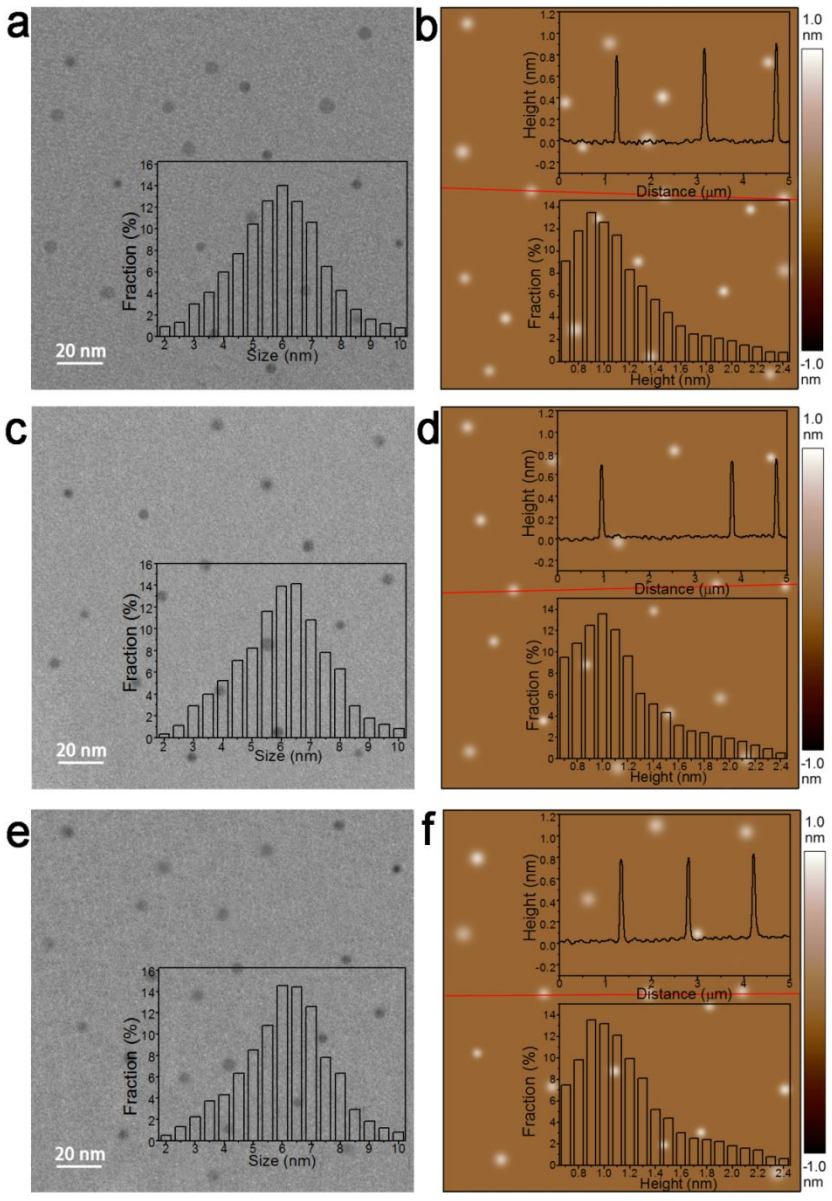

Figure S11. TEM (left column) and AFM images of doped GQDs. (a) Average diameter of N-GQDs is 5.76 ± 1.29 nm (n=126). (b) Average thickness of N-GQDs is 1.28 ± 0.52 nm (n=131). (c) Average diameter of S-GQDs is 5.83 ± 1.48 nm (n=144). (d) Average thickness of S-GQDs is 1.31 ± 0.50 nm (n=150). (e) Average diameter of NS-GQDs is 5.97 ± 1.64 nm (n=167). (f) Average thickness of NS-GQDs is 1.39 ± 0.57 nm (n=145).

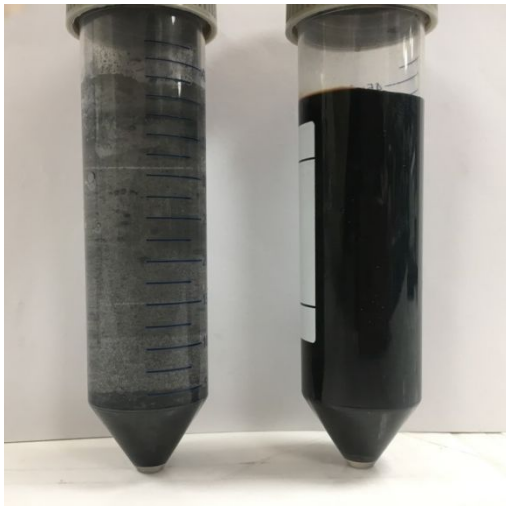

Figure S12. Photographs of graphite suspension without GQDs in H_2O (left) and graphene suspension exfoliated by GQDs (right) after ultrasonication. Graphite power cannot disperse after ultrasonication whereas graphene sheets exfoliated from graphite power by GQDs can stably disperse in water because GQDs can serve as both intercalation agent and surfactant.

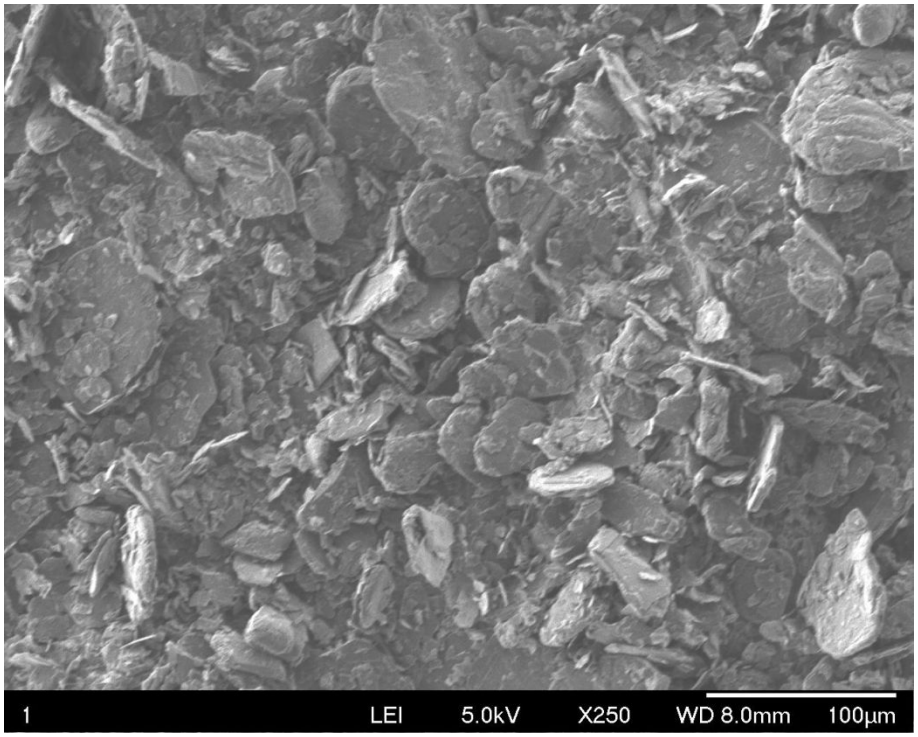

Figure S13. The scanning electron microscope (SEM) image of graphite powder with average particle size of 47.8 ± 3.5 µm (n=146).

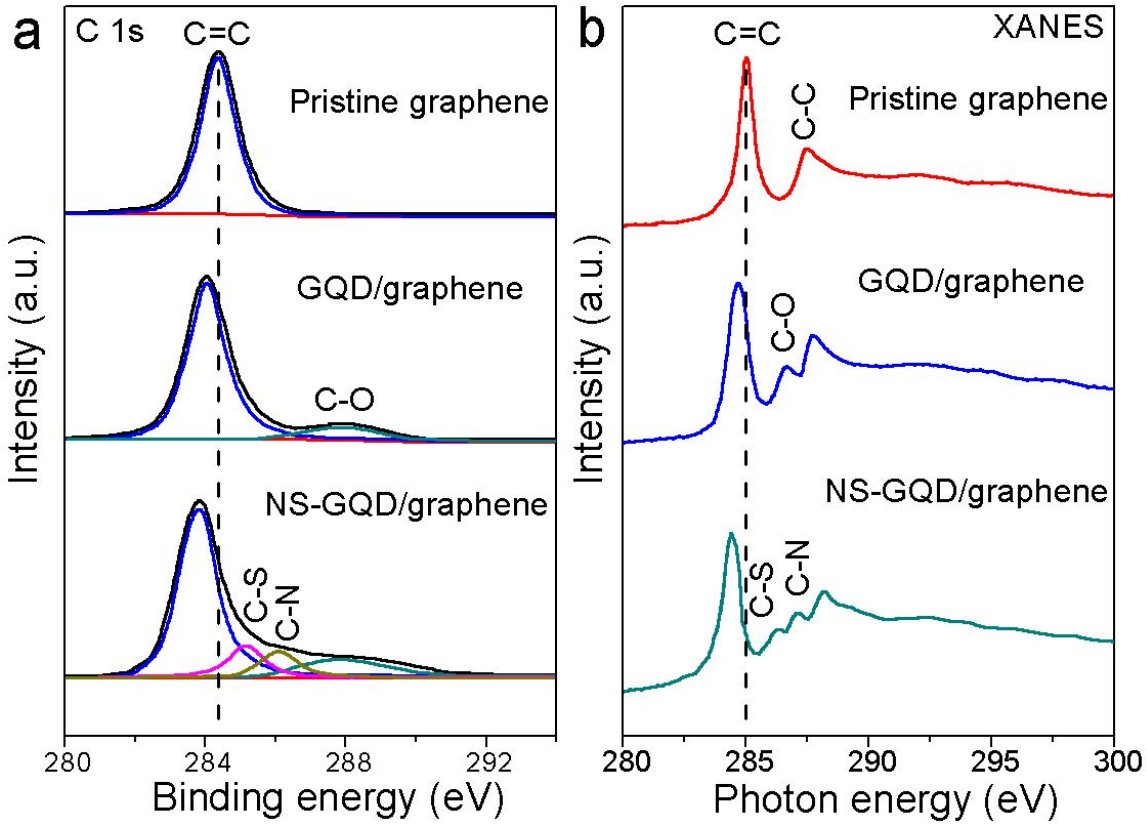

Figure S14. High-resolution C 1s XPS (a) and XANES (b) of pristine graphene (purchased from Sigma-Aldrich, 900394), GQD/graphene vdWH, and NS-GQD/graphene vdWH.

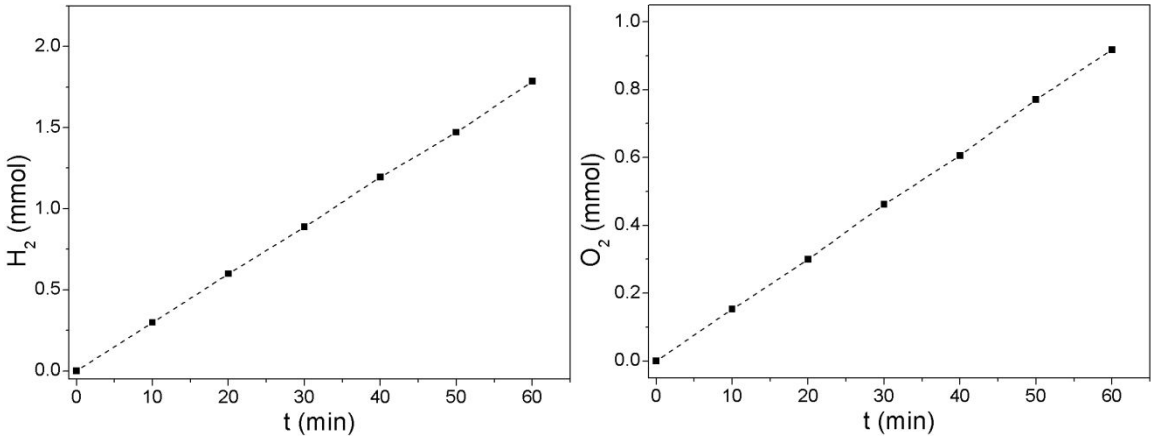

Figure S15. H_2 and O_2 produced from water splitting (in 1 M KOH at a current density of 25 mA cm^{-2}) using NS-GQD/graphene electrodes (2 cm × 2 cm), with a linear fitting (dashed lines). Faradic efficiencies for water splitting HER (or OER) are calculated as the ratio of the amount of produced H_2 (or O_2) gas to the theoretically predicted gas production based on total charge consumed. To prevent leakage, the gas was collected by water drainage strategy.

Table S1 Comparison of the water splitting performance between our NS-GQD/graphene with other advanced photoelectrocatalysts in alkaline media.

Catalyst	Catalyst loading (mg cm^{-2})	Current density (j, $mAcm^{-2}$)	η_{HER} (mV)	H_{OER} (mV)	Ref.
NS-GQD/graphene vdWH	0.125	100	205	237	*This work*
$NiCo_2P_2$/GQD nanosheet array	0.31	100	119	400	[2]
Si/graphene/TiO_2/$FeNiCoO_x$	1.0	10	nil	290	[3]
α-Fe_2O_3/graphene	1.6	3	nil	400	[4]
Ni_5Fe_1/graphene	1.02	10	nil	230	[5]
Sn,Zr-Fe_2O_3-NiOOH	all	2.5	nil	420	[6]
$Co(OH)_x/Bi_2WO_6$	all	1	nil	80	[7]
3D $Fe(PO_3)_2/Ni_2P$	8	10	nil	177	[8]
Co_2P/Carbon	2.5	10	nil	281	[9]
N-doped ZnO nanowires	all	1.4	nil	20	[10]
Sn-doped hematite nanowires	all	2	nil	370	[11]
α-Fe_2O_3 particles	all	5	nil	300	[12]
$NiFeO_x$/haematite	all	1.5	nil	270	[13]
Aligned Ta_3N_5 Nanorod	all	6	nil	195	[14]
Si microwire arrays	all	10	50	nil	[15]
Si nanowires	all	10	380	nil	[16]
cobalt-sulfide film	all	2	85	nil	[17]
ZnO/CuO heterojunction branched nanowires	all	0.16	400	nil	[18]

Table S2 Comparison of the water splitting performance between our NS-GQD/graphene and other all-carbon materials.

Catalyst	Catalyst loading (mg cm^{-2})	Current density (j, $mAcm^{-2}$)	η_{HER} (mV)	H_{OER} (mV)	Ref.
NS-GQD/graphene vdWH	0.125	100	205	237	*This work*
3D nanostructured carbon supported on graphene foil	all	10	260	320	[19]
N,S-doped carbon nanotubes	all	10	450	360	[20]
N, S co-doped graphitic sheets	0.71	10	300	230	[21]
N,S-codoped porous graphene	all	20	300	nil	[22]
N,P-codoped carbon networks	all	30	210	nil	[23]

References for Supporting Information

1. Weissman, S.; Townsend, J.; Paul, D. E.; Pake, G., Hyperfine Splittings in the Paramagnetic Resonances of Free Radicals. *J. Chem. Phys.* **1953,** *21*, 2227-2228.
2. Tian, J.; Chen, J.; Liu, J.; Tian, Q.; Chen, P., Graphene Quantum Dot Engineered Nickel-Cobalt Phosphide as Highly Efficient Bifunctional Catalyst for Overall Water Splitting. *Nano Energy* **2018,** *48*, 284-291.
3. Li, C.; Xiao, Y.; Zhang, L.; Li, Y.; Delaunay, J.-J.; Zhu, H., Efficient Photoelectrochemical Water Oxidation Enabled by an Amorphous Metal Oxide-Catalyzed Graphene/Silicon Heterojunction Photoanode. *Sustainable Energy Fuels* **2018,** *2*, 663-672.
4. Yoon, K.-Y.; Lee, J.-S.; Kim, K.; Bak, C. H.; Kim, S.-I.; Kim, J.-B.; Jang, J.-H., Hematite-Based Photoelectrochemical Water Splitting Supported by Inverse Opal Structures of Graphene. *ACS Appl. Mater. Inter.* **2014,** *6*, 22634-22639.
5. Youn, D. H.; Park, Y. B.; Kim, J. Y.; Magesh, G.; Jang, Y. J.; Lee, J. S., One-Pot Synthesis of NiFe Layered Double Hydroxide/Reduced Graphene Oxide Composite as an Efficient Electrocatalyst for Electrochemical and Photoelectrochemical Water Oxidation. *J. Power Sources* **2015,** *294*, 437-443.
6. Tamirat, A. G.; Su, W.-N.; Dubale, A. A.; Chen, H.-M.; Hwang, B.-J., Photoelectrochemical Water Splitting at Low Applied Potential Using a NiOOH Coated Codoped (Sn, Zr) α-Fe_2O_3 Photoanode. *J. Mater. Chem. A* **2015,** *3*, 5949-5961.
7. Dong, G.; Hu, H.; Wang, L.; Zhang, Y.; Bi, Y., Remarkable Enhancement on Photoelectrochemical Water Splitting Derived from Well-Crystallized Bi_2WO_6 and Co (OH) x with Tunable Oxidation State. *J. Catal.* **2018,** *366*, 258-265.
8. Zhou, H.; Yu, F.; Sun, J.; He, R.; Chen, S.; Chu, C.-W.; Ren, Z., Highly Active Catalyst Derived from a 3D Foam of Fe $(PO_3)_2/Ni_2P$ for Extremely Efficient Water Oxidation. *PNAS.* **2017,** *114*, 5607-5611.
9. Ke, Z.; Wang, H.; He, D.; Song, X.; Tang, C.; Liu, J.; He, L.; Xiao, X.; Jiang, C., Co2P Nanoparticles Wrapped in Amorphous Porous Carbon as an Efficient and Stable Catalyst for Water Oxidation. *Front. Chem.* **2018,** *6*, 580.
10. Yang, X.; Wolcott, A.; Wang, G.; Sobo, A.; Fitzmorris, R. C.; Qian, F.; Zhang, J. Z.; Li, Y., Nitrogen-Doped ZnO Nanowire Arrays for Photoelectrochemical Water Splitting. *Nano Lett.* **2009,** *9*, 2331-2336.
11. Ling, Y.; Wang, G.; Wheeler, D. A.; Zhang, J. Z.; Li, Y., Sn-Doped Hematite Nanostructures for Photoelectrochemical Water Splitting. *Nano Lett.* **2011,** *11*, 2119-2125.
12. Warren, S. C.; Voïtchovsky, K.; Dotan, H.; Leroy, C. M.; Cornuz, M.; Stellacci, F.; Hébert, C.; Rothschild, A.; Grätzel, M., Identifying Champion Nanostructures for Solar Water-Splitting. *Nat. Mater.* **2013,** *12*, 842.
13. Jang, J.-W.; Du, C.; Ye, Y.; Lin, Y.; Yao, X.; Thorne, J.; Liu, E.; McMahon, G.; Zhu, J.; Javey, A.; Guo, J.; Wang, D., Enabling Unassisted Solar Water Splitting by Iron Oxide and Silicon. *Nat. Commun.* **2015,** *6*, 7447.
14. Li, Y.; Takata, T.; Cha, D.; Takanabe, K.; Minegishi, T.; Kubota, J.; Domen, K., Vertically Aligned Ta_3N_5 Nanorod Arrays for Solar-Driven Photoelectrochemical Water Splitting. *Adv. Mater.* **2013,** *25*, 125-131.
15. Boettcher, S. W.; Warren, E. L.; Putnam, M. C.; Santori, E. A.; Turner-Evans, D.; Kelzenberg, M. D.; Walter, M. G.; McKone, J. R.; Brunschwig, B. S.; Atwater, H. A.; Lewis, N. S., Photoelectrochemical Hydrogen Evolution Using Si Microwire Arrays. *J. Am. Chem. Soc.* **2011,** *133*, 1216-1219.
16. Oh, I.; Kye, J.; Hwang, S., Enhanced Photoelectrochemical Hydrogen Production from Silicon Nanowire Array Photocathode. *Nano Lett.* **2012,** *12*, 298-302.

17. Sun, Y.; Liu, C.; Grauer, D. C.; Yano, J.; Long, J. R.; Yang, P.; Chang, C. J., Electrodeposited Cobalt-Sulfide Catalyst for Electrochemical and Photoelectrochemical Hydrogen Generation from Water. *J. Am. Chem. Soc.* **2013,** *135*, 17699-17702.
18. Kargar, A.; Jing, Y.; Kim, S. J.; Riley, C. T.; Pan, X.; Wang, D., ZnO/CuO Heterojunction Branched Nanowires for Photoelectrochemical Hydrogen Generation. *ACS Nano* **2013,** *7*, 11112-11120.
19. Hou, Y.; Qiu, M.; Zhang, T.; Ma, J.; Liu, S.; Zhuang, X.; Yuan, C.; Feng, X., Efficient Electrochemical and Photoelectrochemical Water Splitting by a 3D Nanostructured Carbon Supported on Flexible Exfoliated Graphene Foil. *Adv. Mater.* **2017,** *29*, 1604480.
20. Qu, K.; Zheng, Y.; Jiao, Y.; Zhang, X.; Dai, S.; Qiao, S.-Z., Polydopamine-Inspired, Dual Heteroatom-Doped Carbon Nanotubes for Highly Efficient Overall Water Splitting. *Adv. Energy Mater.* **2017,** *7*, 1602068.
21. Hu, C.; Dai, L., Multifunctional Carbon-Based Metal-Free Electrocatalysts for Simultaneous Oxygen Reduction, Oxygen Evolution, and Hydrogen Evolution. *Adv. Mater.* **2017,** *29*, 1604942.
22. Ito, Y.; Cong, W.; Fujita, T.; Tang, Z.; Chen, M., High Catalytic Activity of Nitrogen and Sulfur Co-Doped Nanoporous Graphene in the Hydrogen Evolution Reaction. *Angew. Chem. Int. Edit.* **2015,** *54*, 2131-2136.
23. Zhang, J.; Qu, L.; Shi, G.; Liu, J.; Chen, J.; Dai, L., N, P-Codoped Carbon Networks as Efficient Metal-Free Bifunctional Catalysts for Oxygen Reduction and Hydrogen Evolution Reactions. *Angew. Chem. Int. Edit.* **2016,** *55*, 2230-2234.